

Open Rotor Aeroacoustic Installation Effects for Conventional and Unconventional Airframes

Michael J. Czech¹

The Boeing Company, Everett, WA 98204 USA

and

Russell H. Thomas²

NASA Langley Research Center, Hampton, VA 23681 USA

As extensive experimental campaign was performed to study the aeroacoustic installation effects of an open rotor with respect to both a conventional tube and wing type airframe and an unconventional hybrid wing body airframe. The open rotor rig had two counter rotating rows of blades each with eight blades of a design originally flight tested in the 1980s. The aeroacoustic installation effects measured in an aeroacoustic wind tunnel included those from flow effects due to inflow distortion or wake interaction and acoustic propagation effects such as shielding and reflection. The objective of the test campaign was to quantify the installation effects for a wide range of parameters and configurations derived from the two airframe types. For the conventional airframe, the open rotor was positioned in increments in front of and then over the main wing and then in positions representative of tail mounted aircraft with a conventional tail, a T-tail and a U-tail. The interaction of the wake of the open rotor as well as acoustic scattering results in an increase of about 10 dB when the rotor is positioned in front of the main wing. When positioned over the main wing a substantial amount of noise reduction is obtained and this is also observed for tail-mounted installations with a large U-tail. For the hybrid wing body airframe, the open rotor was positioned over the airframe along the centerline as well as off-center representing a twin engine location. A primary result was the documentation of the noise reduction from shielding as a function of the location of the open rotor upstream of the trailing edge of the hybrid wing body. The effects from vertical surfaces and elevon deflection were also measured. Acoustic lining was specially designed and inserted flush with the elevon and airframe surface, the result was an additional reduction in open rotor noise propagating to the far field microphones. Even with the older blade design used, the experiment provided quantification of the aeroacoustic installation effects for a wide range of open rotor and airframe configurations and can be used with data processing methods to evaluate the aeroacoustic installation effects for open rotors with modern blade designs.

Nomenclature

AFT	=	or A, aft rotor of a two rotor system
AZI	=	azimuthal directivity angle, degrees
BPF	=	blade passage frequency
BWB	=	Blended Wing Body, specific to Boeing concepts
c	=	chord of wing or vertical or horizontal stabilizer
D	=	diameter of rotor
dB	=	decibel
EPNL	=	effective perceived noise level, decibels
EMANG	=	emission angle, degrees
FWD	=	or F, forward rotor of a two rotor system

¹ Aeroacoustics Engineer, Boeing Commercial Airplanes, AIAA Member, Michael.J.Czech@Boeing.com

² Senior Research Engineer, Aeroacoustics Branch, MS 461, AIAA Senior Member, Russell.H.Thomas@NASA.gov

f	=	frequency (Hz)
<i>HWB</i>	=	Hybrid Wing Body, generic term
<i>LSAF</i>	=	Low Speed Aeroacoustic Facility, Boeing
M_T	=	Wind Tunnel Mach Number
NPR	=	nozzle pressure ratio, used for pylon blowing
<i>PAA</i>	=	Propulsion Airframe Aeroacoustics
PHI	=	polar directivity angle, degrees, downstream axis at 180 degrees
<i>SPL</i>	=	sound pressure level
TNSPL	=	sound pressure level of an identified tone

I. Introduction

OPEN rotor aircraft propulsion systems (two contra-rotating blade rows with no bypass nacelle) have long held the potential to produce a step change to higher propulsive efficiency and, therefore, reduced fuel burn. This is a result of effective bypass ratios upwards of thirty compared to advanced ducted turbofan engines that may reach bypass ratios of 14 to 18 by 2025. The open rotor achieves this high efficiency while reaching cruise Mach numbers of about 0.8, acceptable for modern commercial transports. The correlation of research effort and the price of oil highlights in some way the level of interest in the potential of the open rotor propulsion system.

The first wave of research and development effort took place after the oil price shocks of the 1970s and 1980s. General Electric worked in cooperation with NASA Lewis Research Center (now Glenn Research Center) to develop the UDF[®] demonstrator engine. This demonstrator engine was flight tested on an MD-80 in collaboration with McDonnell Douglas¹. In collaboration with Boeing, the UDF[®] was flight tested on a Boeing 727-100 airframe starting in 1986². The demonstrator engine used an open rotor system including a forward and an aft set of blades, each with eight blades (8 by 8) and using a blade shape design designated the F7/A7. This successful flight test established the viability of the open rotor, demonstrated integration with the test aircraft, system operability, rotor stability, and cruise performance in good agreement with predictions. Acoustic measurements were also acquired during the flight test for community noise, cabin noise as well as enroute noise, all three of significant concern for an engine without the noise reducing advantages of a bypass nacelle and acoustic liner technology to attenuate the rotor-rotor source noise.

In the same timeframe of the late 1980s and early 1990s Boeing studied a design for a twin engine, tail mounted, single aisle transport, the 7J7. General Electric also developed the design of an open rotor engine that could be applied to the 7J7 and designated the GE36. The GE36 included a more advanced rotor design with higher aerodynamic performance and reduced noise from improved blade design and an unequal number of blades on the forward and aft rows. Many factors probably contributed to the fact that the 7J7 was not offered as an aircraft product. Certainly one factor was the sharp drop in oil prices in the 1990s together with relatively high levels of noise compared to competing turbofan engines^{3,4}.

With the next significant and sustained rise in oil prices that began in 2007 came renewed interest in the open rotor together with the prospect of applying the improvements of all the technological advancements since the 1990s including higher fidelity 3D computational fluid dynamics. New research efforts began both in the United States and in Europe. Van Zante⁵ summarizes a collaborative effort between NASA, General Electric, and the FAA that tested several new rotor designs for low speed noise and high speed performance. Modern rotor designs have demonstrated large reductions in source noise while retaining high propulsive efficiency. Van Zante⁵ and Guynn et al⁶ also present predicted results for the fuel burn and community noise for a single aisle aircraft with tail mounted open rotor engines updated to a 2020 timeframe technology and used, for rotor source noise, the wind tunnel results from the test campaign reported in Van Zante⁵. The predicted cumulative noise margin relative to stage 4 is reported at 13 dB and clearly demonstrates the significant advancements in open rotor blade design of the last three decades. At the same time open rotor propulsion systems have comparatively higher noise levels and greater installation challenges compared to turbofan engines on an equal thrust basis. One major component impacting both is the engine pylon.

The pylon installation effect has been the subject of considerable research^{5,7} together with noise reduction strategies and was found to enhance inflow distortion that leads to higher noise levels. Blowing from the pylon trailing edge that fills in the wake of the pylon has been shown to be an effective technology to mitigate the noise increase from a pylon when located in front of the open rotor, a pusher configuration.

Beyond the pylon and angle of attack effects there have been very few other studies on the aeroacoustic installation effects of open rotors from additional airframe elements. Shivashankara et al⁸ included a fuselage section with a T-tail empennage and determined the increase in the front rotor BPF due to flow distortion. In the recent era of research, Van Zante⁵ also mentions studies, separately with Boeing and Airbus, that used influence bodies in proximity to the open rotor to simulate the flow distortion from a fuselage. Aircraft system noise includes many propulsion airframe aeroacoustic (PAA) installation effects from flow distortion and acoustic propagation effects that can be highly dependent or vary in importance based on specific aircraft configuration options. Typically these effects result in increases in noise at the aircraft system level.

Aircraft concepts with open rotor propulsion systems have been studied and the two types of configurations shown in Figure 1 have received considerable attention. The tail mounted configuration similar to that tested in the earlier flight test demonstration represents one of the classic open rotor configurations considered with a tube and wing airframe. While the tail mounting minimizes cabin noise challenges there can be acoustic scattering from the T-tail empennage⁸. The other classic configuration is a high wing with open rotors in a puller mode. This



Figure 1. Two possible configurations of tube-and-wing airplane architecture with open rotor engines. Images are reproduced with the permission of The Boeing Company, copyright © The Boeing Co., 2010.



Figure 2. A notional image of a Boeing Blended Wing Body aircraft concept with open rotor propulsion studied under a NASA contract, Bonet et al¹¹. Image reproduced with the permission of The Boeing Company.

configuration can have strong acoustic installation effects as the wing upwash increases the flow distortion into the rotor and this leads to higher noise levels. The open rotor sound field scatters off of the fuselage and wing and, in addition, cabin noise is expected to require additional measures. Determining the aerodynamic installation effects of these two classic configurations continues to be a challenge⁹ and the subject of recent research. There are also other aircraft configuration possibilities with a tube and wing airframe that may be attractive if the information is available so that system trades can be determined¹⁰. Unconventional aircraft configurations such as the hybrid wing body (HWB), Figure 2, have been studied by NASA and Boeing and also represents a possible configuration where shielding of propulsion noise can be a significant community noise reduction approach¹¹.

Looking to the future, turbofan engine technology continues to advance and remains the propulsion system of choice for commercial air transport. In addition, requirements for further aircraft noise reduction from regulations and local airports is expected to continue. To apply a new technology such as the open rotor, reducing uncertainty is essential in the trade studies for total aircraft system performance¹². As part of the total aircraft system trade study, the determination of PAA installation effects with higher confidence are essential in aircraft system noise predictions, influencing aircraft configurations options, and in achieving additional noise reduction.

Given the importance of the ability to refine both conventional configurations and to explore unconventional aircraft configuration possibilities, NASA and Boeing collaborated on an exploratory experimental study including a broader range of PAA installation effects for the open rotor, noise reduction technologies, and aircraft configurations. The objectives were to provide understanding and quantification of a range of PAA installation effects, validation data for prediction methods and, data that could be used to support aircraft system level noise assessments. Some initial experimental results for this test campaign were presented earlier¹³ and are now reported in more complete form. Companion papers by Bahr et al¹⁴ and Guo et al¹⁵ show how the data has been processed to be applied to aircraft system level assessments of HWB concepts that are reported by Thomas et al¹⁶ and Guo et al¹⁷.

II. Experimental Method

A. Facility

The experimental campaign was conducted in the Boeing Low Speed Aeroacoustics Facility (LSAF), shown in Figure 3. A 9 by 12 ft open jet is used to produce the forward flight simulation with low background noise levels and with a maximum Mach number of 0.25 for this experimental setup. Figure 3 shows the basic setup for this

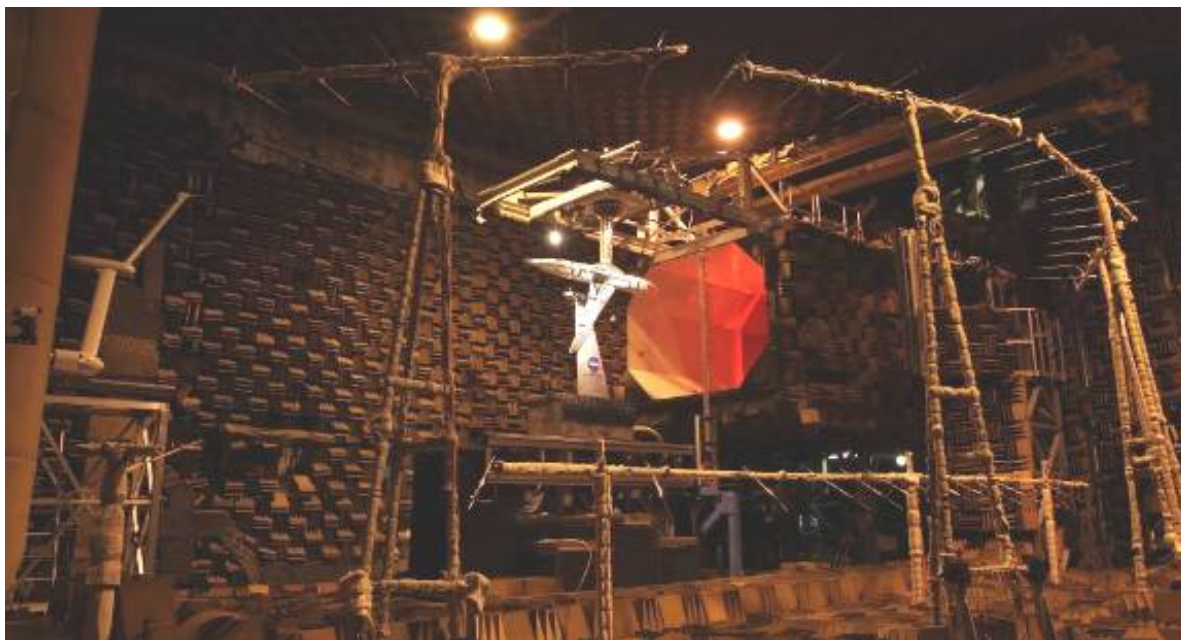


Figure 3. Boeing Low Speed Aeroacoustics Facility configured for open rotor testing in late 2010.

campaign with the airframe attached to an overhead structure and the open rotor rig attached to an aerodynamically shaped strut from below the open jet. The Boeing LSAF facility has the capability to remotely control the

positioning of the airframe relative to the open rotor with an estimated accuracy of 0.1 inch allowing the spacing between rotor and airframe to be investigated efficiently over a wide range of values. Both the open rotor rig and the airframe could be rotated manually to investigate angle of attack effects. The facility is also equipped with a traversing phased array system to cover polar angles from 50 to 150 degrees. The phased array is stowed upstream of the wind tunnel exit when not in use. A flow measurement system shown in a downstream location could be remotely controlled and was typically stowed upstream of the wind tunnel exit to prevent acoustic interference effects. Far field microphone arrays are also visible in Figure 3, two arrays, one polar and one sideline, at two azimuthal angles. The bulk of the acoustic data was obtained by the inflow traversing array of microphones shown in Figure 3 positioned upstream of the model and just at the exit of the wind tunnel.

B. Open Rotor Rig

The forward and aft rotors were driven by compressed air powered turbines and both rotors included eight blades. The strut supporting the open rotor model is shown in Figure 4 where the model pylon was painted in black and the lower aluminum part was referred to as the support strut. The strut accommodated all supply, control and exhaust lines for the model. The high pressure air driving the turbines was ducted into the open rotor rig and then exhausted back out through the support strut in a complex piping system. The exhaust air was then ducted through the roof of the LSAF to prevent contaminating noise measurements with exhaust noise. The support strut was designed to be as slender as possible with a small footprint to reduce acoustic and aerodynamic interference. The close-out of the strut was very aggressive and vortex generators were implemented to minimize flow separation at the trailing edge.



Figure 4. Open rotor rig mounted on support strut.

There was only one set of blades used for this test and they are referred to as F7/A7. These blades were tested at two different pitch angles of 30.8/31.6 degrees for static conditions and 38.0/37.2 degrees for Mach numbers greater than 0.2. A spare set of blades for the front and aft rotor was fabricated in case of blade failure during the test. Since no blade failure occurred the spare set was not used. The contra-rotating, eight by eight, open rotor used in this experiment was legacy technology from the 1980s flight test project. It was chosen for this experiment because it was existing hardware available in the timeframe necessary for this experiment and results could be correlated with model and full-scale information from the tests of the 1980s. Although modern blade designs are significantly quieter key aeroacoustic features regarding tone generation as well as propagation are independent of the blade design allowing for the development of prediction models to bridge the gap in blade design advances. While comparatively small in size with a 12 inch rotor diameter this size does allow for installed testing with different airframes at scales than can be efficiently managed at LSAF. In addition, the rotor at this scale allowed the usage of an existing high lift aerodynamic airframe model at appropriate scales for the chosen rotor. Taken all together, this combination represented a good choice in experimental design to support the objectives of the effort.

The testing was conducted with the rotor configured in a pusher configuration which could not be changed during testing. The flow distortion created by the pylon was expected to increase the noise levels at blade passage frequencies and its harmonics primarily for the front rotor. The influence of the pylon wake was mitigated through pylon edge blowing for conditions of interest. While the pusher configuration was seen as the preferred configuration for both tail mounted installations and perhaps mid fuselage installations it is not considered desirable in a forward of the wing location.

The open rotor was operated over a thrust range covering both typical approach and takeoff requirements. The majority of the conditions were such that the aft rotor was spun about 10% faster than the front rotor to decouple rotor only and interaction tones. Data was acquired predominantly at a flow speed of $M_T=0.24$ with some additional data points at lower Mach numbers.

C. Acoustic Instrumentation

Both inflow and out-of-flow microphones were used to describe the characteristics of the open rotor acoustic field. An inflow microphone array was installed 36 inches (3 rotor diameters) away from the blade tips when positioned in line with the front rotor plane. The inflow array is visible in Figure 4 just upstream of the support strut. Overall 13 microphones were mounted on a vertical sting covering azimuthal angles from +45 to -45 degrees relative to the open rotor horizontal. The microphones had Brüel&Kjær nose cones of the type UA0385 to reduce flow noise and were mounted on streamlined holders. The inflow microphones were mounted on a vertical sting which was connected to a traversing mechanism allowing the measurement of microphone angles from 30 to 150 degree polar. A typical traverse would cover this range in 10 degree increments coming to a full stop at every angle before data was taken. It required approximately 8 minutes to complete one full polar traverse.

The data acquired by out-of flow microphones suffered from the scattering effect of the tunnel shear layer that result in a haystacking effect of the rotor tones. This effect increased with frequency and made the interpretation of tonal data challenging. All open rotor data reported in this study will be with the inflow array unless otherwise noted.

Brüel&Kjær Type 4939 microphones were used for out-of-flow free-field measurements. The microphones are set at normal incidence and without the protective grid, which yields a flat frequency response up to 100 kHz. A 25 feet polar array was used where the microphones were spaced in 5 degree increments from 50 to 150 degrees. In addition, a 60 degree array at a sideline distance of 21 feet was utilized to help understand the azimuthal variation of open rotor noise in the far-field. The microphone locations are provided in tunnel coordinates.

The test also included the use of airframe mounted surface kulites and a traversing phased array system. The data from these systems will not be reported in this paper.

D. Flow Measurements

A flow measurement system was used extensively to measure the steady state flow field near the rotor with a total pressure and total temperature probe. The flow measurement system is shown in Figure 5. The system was comprised of two arms which are driven by servo motors to sweep a 5-hole total pressure probe through the flow field of interest. The overall range of the system was 132 inches.

The downstream flow field of the plume was measured for CFD validation purposes and to support rotor performance assessment. This system was also deployed to characterize the effectiveness of the blowing pylon.

The boundary layer near the airframe trailing edge was assessed with a rake that included 16 total pressure probes spaced non-linearly over a 3 inch height.

E. Airframe Configurations

The test program was concerned with open rotor installation effects with both a conventional tube and wing airframe and a hybrid wing body configuration. The conventional airframe had a wing span of approximately 12 feet and was a representative model of a large commercial airplane and is shown in Figure 6a. This airframe model was equipped with at high lift leading edge and trailing edge system. For each airframe a large number of positions were investigated and, in the case of the tube and wing airframe, this included both installations near the tail and around the wing. As seen in Figure 6a, the pylon is not attached to the airframe and is, in fact, at an orientation other than it would be if it were attached to the airframe. This experimental configuration was chosen because of what was considered to be a net favorable trade-off. While the pylon does create an azimuthal directivity effect that is not in the correct orientation for an actual installation, the azimuthal pattern from this experimental configuration is held constant by this mounting off of the support strut. By not attaching the open rotor to the airframe, the relative spacing between the rotor and airframe can be repositioned remotely during experimental operation allowing a very large increase in the test productivity and the measurement of a much larger range of parameters and configurations than would otherwise be



Figure 5. Quantitative Wake Survey System for flow measurements.

possible. The positions tested with a tube and wing airframe in the over-the-wing sub-set of positions are shown in Figure 6b and indicated by numbers P1 through P4. The position P4, shown in this figure, indicates the location of the center point between the front and aft rotor and is 1D upstream of the wing trailing edge.

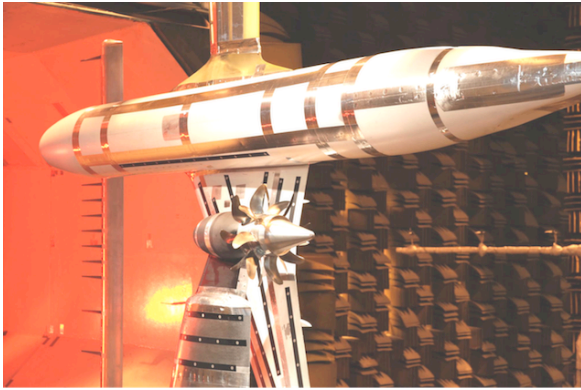


Figure 6a. Configuration for the open rotor in proximity to the main wing. Inflow traverse seen upstream of the model.

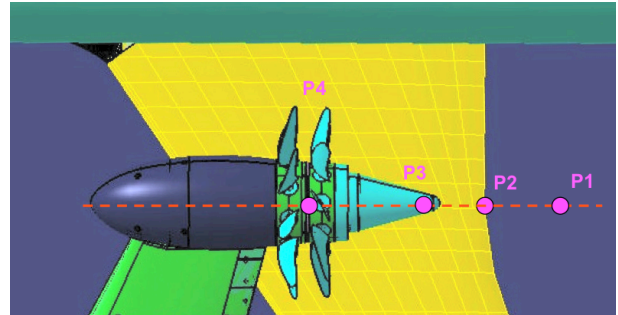


Figure 6b. Schematic of the rotor in the over-the-wing configuration relative to the main wing of the conventional airframe. Positions of the open rotor relative to the trailing edge of the main wing.



Figure 7. Experimental configuration for a notional U-tail tube and wing aircraft concept. The U-tail has a vertical surface at the tip of the horizontal surface.

Figure 7 shows one of the open rotor installations at the aircraft tail. Several axial locations, not illustrated here, were investigated to better understand sensitivities to this configuration. A conventional tail, a T-tail, and the U-tail shown in Figure 7 were all tested. The U-tail shown in Figure 7 was intentionally oversized in order to provide some possibility of providing a significant amount of noise reduction from shielding. Providing noise reduction from shielding appears to be a challenge for tail mounted configurations that have been proposed in recent years. The picture also illustrates the range of azimuthal angles covered during the test. The azimuthal angle of 0 deg represents a flyover observation location and the results in this study are reported at this angle unless otherwise noted.

A HWB airframe model, shown in Figure 8, was manufactured at an 8% scale with respect to a possible half-scale demonstrator aircraft (~120ft span) studied by NASA at the time. The model planform was derived from the Boeing BWB-450 airframe¹⁸ and had NACA airfoils as leading and trailing edges. The maximum model chord was 60 inches and it was clipped in the spanwise direction to accommodate the model in the tunnel without excessive shear layer interference. Two different verticals were built for this model and the verticals could be installed at two different inclination angles. The model elevons could be deflected to angles of 0, -5 (up) and +5 (down) degrees.

The majority of HWB open rotor installations focused on simulating a twin-powered configuration and studying sensitivities to axial location as well as the presence of the verticals as shown in Figure 8. The reference point for axial movement was defined such that the center point between the rotors was at the wing trailing edge. The most downstream location was 0.5 fan diameters (D) downstream of the reference point and two fan diameters was the furthest upstream location. Figure 9 shows the rotor at 1D upstream of the trailing edge at the spanwise location for the twin engine configuration. The outer bounds of this axial range were of little practical interest but were included to enhance the understanding of shielding effects with little impact on test time due to the highly efficient airframe movement. Figure 9 also shows an installation with the HWB verticals that presented a physical barrier for measuring locations at the wing trailing edge or further downstream with the vertical in place. However, the key installations of interest at about 1D or greater upstream of the trailing edge could be measured in this set-up with

vertical present. The test included two vertical designs that differed in overall size and the cant angle was also changed in the test. The HWB airframe had a removable panel in the main wing and on both elevons where either kulites or acoustic lining elements could be installed flush as shown. Figure 9 shows one of the acoustic liners installed in all three pockets. This is one of three acoustic liner designs¹⁹ provided by NASA Langley Research Center for this experiment. All three liners targeted the frequency range including BPF and 2 BPF. The liner shown is designated the broadband liner and is filled with a Nomex™ material.

F. Broadband Noise Source

To support the overall objectives of the test campaign, a broadband point noise source was also tested after the open rotor. An image of the broadband noise source is shown in Figure 10 where broadband noise is generated by four jetlets impinging at a point. The figure also shows the fairing that was designed to simulate the insertion loss and directivity effect with the broadband noise source installed in a nacelle.

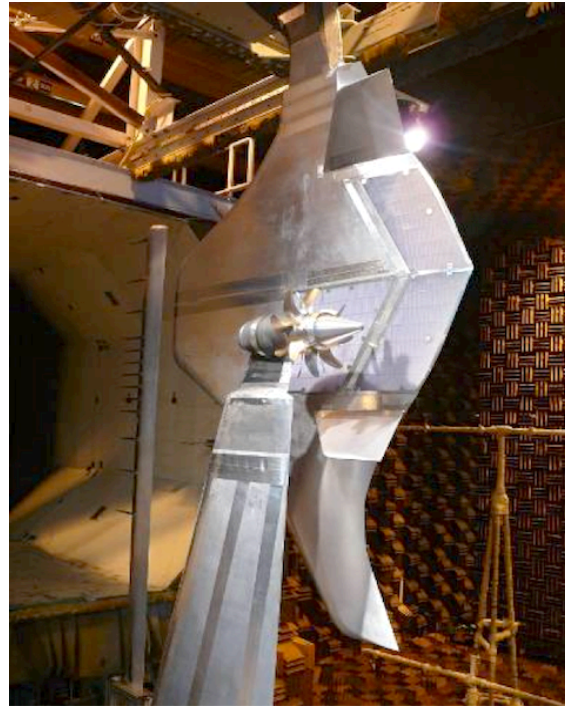


Figure 8. Experimental configuration representative of the Hybrid Wing Body configuration including vertical stabilizer surfaces.

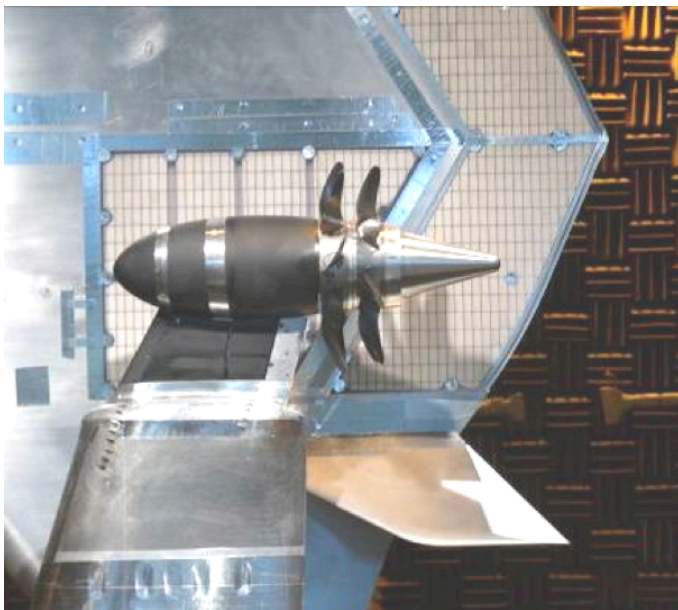


Figure 9. Close up of the HWB experimental configuration. A vertical surface is shown as well as the inserts on each elevon and a third airframe insert that the open rotor is positioned over. The solid inserts could be replaced with acoustic lining or with instrumented inserts.



Figure 10. Broadband point noise source without nacelle (left) and with nacelle (right).

III. Results

Figure 11 shows a spectrum acquired by the inflow array at 90 degrees polar and at 0 degree azimuthal for an isolated open rotor at high power. The data is corrected for atmospheric effects and normalized to a 20ft polar arc. Since the open rotor had an equal number of front and aft rotor blades the rotors were run intentionally at slightly different speeds. This allowed the engine order tones from each blade row to be uniquely distinguished from rotor alone tones. The figure shows the engine orders for the front rotor on the lower horizontal axis. The aft rotor engine orders are aligned with the upper horizontal axis for easier tone identification. The blade passage tone of the front rotor, 8th engine order, is the first higher-level tone evident in the spectrum with a tone emergence relative to the broadband noise of more than 30dB. The following tone in the spectrum is the aft rotor BPF and it is found to be about 10dB lower than the front rotor one. The figure also illustrates the background levels of the wind tunnel at $M=0.24$ which was the highest speed setting used in this test. The results demonstrate low levels of background noise relative to the open rotor spectra up to high engine orders of 72. The classic blade design clearly offered an advantage here as the contamination of the rotor spectra by wind-tunnel noise could be, for all practical purposes, be ignored.

The main objective of the study was to investigate a large number of configurations and capture spectral increments between those in order to describe effects of shielding, open rotor settings or airframe configuration changes. For that reason it was very important to have low levels of data scatter and a good repeatability of test points. The repeatability of the data at a low power setting is illustrated in Figure 12 where the tone levels of six low order rotor alone and interaction tones are plotted versus emission angle. The data was acquired on different days and the comparison of the results shows a very good repeatability. The data repeated, in general, within 1dB and this was checked a few times throughout the test campaign. Repeatability at high power was similar. The designation 1F0A denotes the fundamental BPF for the front rotor and the first interaction tone between front and aft rotor is given by 1F1A. The fundamental BPF for the aft rotor is described by 0F1A.

The variation of the open rotor acoustic field with polar angle is given in Figure 13 at angles of 50, 90 and 130 degrees with the rotor operating at high power. The spectra are plotted against engine order for the forward and rear rotor to ease characterization of tones. The data at 90 degrees shows fundamental blade passage frequency (BPF) tones for the front and rear rotor tones to be dominant. The third strongest tone in the spectrum is an interaction tone of two front BPF and one aft BPF (2F1A). The rear rotor was spun about 11% faster than the front rotor leading to a correspondingly higher blade passage frequency. Front and aft BPF were found to drop by approximately 12dB at polar angles of 50 and 130 degrees relative to the 90 degrees overhead angle. On the other hand, the interaction tones 2F1A and 1F2A were the loudest at the 130 degree aft angle and show a somewhat smaller sensitivity to polar angle.

Pylon blowing was utilized to mitigate the effect of the upstream pylon on open rotor noise. The effectiveness of the pylon blowing was assessed with an automatic flow measurement system and surveys were conducted both for the pylon with no blowing and different blowing pressure ratios as shown in Figure 14. The results show the axial velocity profile of the pylon wake and the mitigation of this wake through pylon blowing for two different blowing

ratios. The initial wake deficit of up to 50ft/s is reduced to approximately 5ft/s for the higher blowing pressure indicating an effective blowing performance.

The effectiveness of the pylon blowing is shown in Figure 15 and the blowing is found to primarily reduce the pylon rotor interaction tones. The rotor-rotor interaction tones are largely insensitive to the pylon blowing since the dominant mechanism for these tones is the front rotor wake impacting the aft rotor. The first and second harmonic of the front rotor are reduced by 3 to 5dB at aft angles. The rear rotor BPF remains largely unchanged with blowing. It is also noted that the pylon blowing effectiveness degraded with angle of attack.

Figure 16 shows the spectral changes for an installation position where the open rotor is positioned in front of the conventional airframe's main wing. The isolated and installed spectra are plotted at the same SPL level reference. While the blade passage tone of the forward row increases only slightly, the blade passage tone of the aft rotor increases almost 10 decibels and both front and aft 2BPF increase by about 6 decibels. In addition, the broadband level rises by 6 to 10 decibels over the entire frequency range. These findings can be attributed to the increased flow distortion caused by the presence of the wing.

A propulsion unit installation with the conventional airframe at wing mid-chord highlights the potential for rotor noise shielding. This installation can be seen as the limit of what might be achievable, in terms of shielding, with a conventional airframe and would face major engine integration challenges. The results in Figure 17 indicate a 20dB lower fundamental BPF tone relative to the isolated test case. This location also provides a 10dB lower broadband noise level.

Open rotor installation effects were also investigated at the tail of the airplane with both a T-tail and a U-tail configuration. Results for the installation effects of a U-tail configuration are given in Figure 18 where the isolated rotor noise levels are compared to the installed set-up. The rotor was configured as pictured in Figure 7 where the rotor center was at the U-tail leading edge. There is very substantial shielding at angles from about 60 to 120 degrees. The rotor alone tones are particularly well shielded at overhead angles with installation increments of up to 20dB.

The azimuthal variation of the installation effects are quite significant as the acoustic propagation is altered by the presence of the fuselage. This is well illustrated in Figure 19 where the dominant modes for azimuthal angles of 0, +45 and -45 degrees are shown. The fuselage blocks part of the forward radiating noise when observed at an azimuthal angle of +45 degrees. This is seen for the modes 2F0A and the interaction modes 1F1A and 2F1A where significant tone reductions are obtained forward of 90 degrees polar. Interestingly mode 1F0A is found to be louder at the +45 degree azimuth compared to the -45 degree angle. In order to explain this it is informative to take a closer look at the azimuthal variation of the isolated rotor set-up.

Figure 20 shows the both polar and azimuthal characteristics of the isolated rotor set-up for the lowest order modes. The fundamental BPF of the front rotor shows the greatest sensitivity to azimuthal measurement location as the pylon introduces an azimuthally varying distortion. For the mode 1F0A the levels are greater at the +45 degree azimuthal angles compared to the -45 degree one. This may explain the finding from above where the fuselage is still likely to shield some of the fundamental front rotor BPF at +45 degrees. However, this shielding occurs on a tone that is already higher compared to the -45 degree angle in the isolated rotor set-up. The aft rotor only BPF tones as well as the interaction tone show little sensitivity to azimuthal angle.

The BWB airframe has a greater potential for utilizing the airframe as an acoustic shield, in particular in the forward arc. Figure 21 shows the installed open rotor noise with the rotor being one diameter (1D) upstream of the BWB wing trailing edge at 50, 90 and 130 degrees. The airframe had no verticals installed and the elevons were at 0 degrees deflection. The comparison with the isolated rotor spectra shows very significant shielding effects for the front rotor BPF at 50 degrees with a reduction of this tone by 13dB. The aft rotor BPF tone is not shielded and the tone levels even increase slightly possibly due to diffraction effects. In general, both tones and broadband noise, are lowered by about 10dB at the 50 degree polar angle. It is also interesting to note that the spectra shows some haystacks that would be typical for scattering effects of tones by turbulence and may be due to the propagation of the tones through the wake of the airframe. The 90 degree polar arc data demonstrates significant shielding benefits and this is also the case for the aft rotor fundamental blade passage tone. Fewer haystacks are observed at 130 degrees and the shielding benefits for the fundamental BPF tones are insignificant. Interestingly the interaction tones and higher harmonics are still lower by more than 5dB when compared to an isolated set-up.

The sensitivity of the shielding effects to the open rotor position is illustrated in Figure 22 with the rotor positioned at 0, 0.5D and 1D upstream of the HWB trailing edge. When the open rotor unit is positioned at 0 the front rotor is slightly upstream of the trailing edge while the aft rotor is somewhat downstream of the trailing edge. The aft rotor fundamental BPF tone experiences shielding of about 4 to 6dB at overhead angles. This is, somewhat surprisingly, greater than the shielding seen on the front rotor BPF where this effect is closer to 2dB. The 2nd harmonic for the front rotor BPF shows significant shielding of 6 to 10dB at forward angles. The greatest amount of

shielding is observed for the fundamental interaction where the tone levels are about 20dB lower at this rotor installation compared to an isolated set-up.

The sensitivity of the rotor tone shielding to location is clearly evident when examining the results with the rotor at 0.5D. For this location most tones are reduced by 10dB or more at forward to mid angles. There is no shielding at aft angles and some tones even show a slight increase at polar angles greater than 120degrees which might be due to trailing edge diffraction.

The installation at 1D changes the directivity pattern of all tones to an approximately flat behavior meaning the tone levels vary little with polar angle. The shielding benefit is now between 10 and 20dB over most angles apart from the aft arc. Substantial shielding is also achieved for broadband noise.

An acoustic liner using NomexTM material was installed in the HWB wing pocket and the elevons and tested with the open rotor installed at the 1D position as shown in Figure 23. The front rotor fundamental frequency is reduced mostly in the 40 to 60 degrees range where the levels are about 5dB lower with the lining added. The aft rotor fundamental is reduced by 3dB at aft angles and no effect is seen forward of 90 degrees. The greatest lining impact is observed for the interaction tone where levels were attenuated by 4 to 6dB from 80 to 120 degrees.

The boundary layer thickness was altered by adding roughness elements to the airframe model and this increased the boundary layer from approximately 0.5'' to 2.0''. Figure 24 indicates that the low order open rotor tones remain largely unchanged by this alteration and this is likely due to the fact that the open rotor was positioned 3'' from the surface. This would suggest that the flow distortion going into the rotor was not significantly by the boundary layer thickening. It is noted that slight increase in broadband noise was observed.

A second part of the test consisted of using a broadband noise source to better understand PAA effects with regards to a broadband noise source. This could for example be used to investigate the shielding potential of aftfan noise for a turbofan engine. The PAA effects of broadband noise were studied in different configurations where the isolated set-up without the airframe being present was the reference set-up. This was compared to a configuration where a nacelle was added. The third configuration involved the HWB airframe but the nacelle was not present in this case. Figure 25 shows the levels of the broadband noise source for an isolated set-up without nacelle, a set-up with the nacelle and when it was installed at the 1D location with the HWB airframe. The data were acquired with the far-field microphone array and corrected for atmospheric effects and wind-tunnel shear layer. The results show the sensitivity to both the configuration and the polar angle. The influence of the nacelle is limited to 2dB relative to the isolated broadband noise source at both the 60 and 120 degree polar angle. The character of the spectra changed when the nacelle was added and the small humps in the spectra may suggest reflections. The 90 degree results show distinctly lower levels with the nacelle installed as the direct line of sight is blocked.

The broadband noise shielding benefits are greatest at 60 and 90 degrees reaching about 15dB over a broad range of frequencies. While the aft angle shielding effect is reduced to 10dB this is still a very significant number.

IV. Conclusion

An extensive model scale test program was conducted to investigate installation effects on open rotor noise. The study comprised both tests with a conventional airframe and a HWB platform where, in both cases a large number of configurations were tested. The propulsion unit was of similar scale as the airframes and produced thrust levels appropriate for the airframe models tested. The open rotor data was sampled with both an inflow traversing microphone array as well as out-of flow microphones. In addition, flow surveys were conducted to assess the pylon blowing performance and measure the flow fields to support CAA validation studies. The open rotor was tested with a conventional airframe and positioned in several positions forward, over and just downstream of the main wing. In addition, open rotor positions were studied at the tail. The studies included changes in the high lift configuration as well as angle of attack investigations.

The HWB propulsion airframe aeroacoustics were studied extensively with variations in open rotor installations as well as airframe changes. These changes included different deflection of the elevons, the addition of verticals as well as the integration of three different acoustic lining types. Very substantial shielding benefits exceeding 12dB for the most dominant modes were found with the rotor installed 1D upstream of the wing trailing edge. The addition of the lining provided further reductions of about 3dB for certain modes.

While the majority of the experimental study was conducted with an open rotor additional data was acquired with a broadband noise source simulator. This broadband noise source was tested with and without a nacelle in both isolated and installed configurations. With this and the open rotor noise data base an extensive data set was obtained

that provides valuable guidance for both tool development as well as system level assessments for a wide range of configurations.

Acknowledgments

The authors thank the NASA Environmentally Responsible Aviation Project, Dr. Fay Collier, Project Manager, for funding this research. The Boeing Aero/Noise/Propulsion Laboratory and the Low Speed Aeroacoustics Facility staff in particular are thanked for the many contributions required to successfully refurbish the Boeing Open Rotor Rig and complete the ambitious wind tunnel test campaign for this research. Dr. Incheoe Lee's support in the test conduct, data analysis, and documentation is greatly appreciated.

References

- ¹Nichols, H.E., "UDFTM Engine / MD-80 Flight Test Program," AIAA 88-2805, 1988.
- ²Harris, R.W., and Cuthbertson, R.D., "UDFTM/727 Flight Test Program," AIAA Paper 87-1733, 1987.
- ³Blythe, A.A., and Smith, P., "Prospects and Problems of Advanced Open Rotors for Commercial Aircraft," AIAA Paper 85-1191, 1985.
- ⁴Conlon, J.A., and Bowles, J.V., "Application of Advanced High Speed Turboprop Technology for Future Civil Short-Haul Transport Aircraft Design," AIAA Paper 78-1487, 1978.
- ⁵Van Zante, D.E., "The NASA Environmentally Responsible Aviation Project / General Electric Open Rotor Test Campaign," AIAA Paper 2013-415, January, 2013.
- ⁶Guynn, M.D., Berton, J.J., Haller, W.J., Hendricks, E.S., and Tong, M.T., "Performance and Environmental Assessment of an Advanced Aircraft with Open Rotor Propulsion," NASA TM-2012-217772, October, 2012.
- ⁷Ricouard, J., Julliard, E., Omais, M., Regnier, V., Parry, A.B., and Baralon, S., "Installation Effects on Contra-rotating Open Rotor Noise," AIAA Paper 2010-3795, June, 2010.
- ⁸Shivashankara, B., Johnson, D., Cuthbertson, R., "Installation Effect on Counter Rotation Propeller Noise," AIAA Paper 90-4023, October, 1990.
- ⁹Aschwanden, P., Muller, J., Griffiths, R.C., Smith, B., and Northall, R., "Wind Tunnel Testing of a Counter Rotating Open Fan Powered Aircraft," AIAA Paper 2012-2860, June, 2012.
- ¹⁰Mann, S.A.E., and Stuart, C.A., "Advanced propulsion through the 1990s: An Airframers View," AIAA Paper 85-1192, 1985.
- ¹¹Bonnet, J.T., Schellenger, H.G., Rawdon, B.K., Elmer, K.R., Wakayama, S.R., Brown, D.L., and Guo, Y., "Environmentally Responsible Aviation Project N+2 Advanced Vehicle Concepts Study and Conceptual Design of Subscale Test Vehicle, Final Report," final report for NASA Contract NND11AG03C, to be published.
- ¹²Barrie, D., Norris, G., and Wall, R., "Open Question," Aviation Week and Space Technology, October 22, 2007, pp. 26-27.
- ¹³Czech, M.J., and Thomas, R.H., "Experimental Studies of Open Rotor Installation Effects," AIAA-2011-4047, invited presentation at the 3rd AIAA Atmospheric and Space Environment Conference, June, 2011.
- ¹⁴Bahr, C.J., Thomas, R.H., Lopes, L.V., Burley, C.L., and Van Zante, D.E., "Open Rotor Tone Shielding Methods for System Noise Assessments Using Multiple Databases," 52nd AIAA Aerospace Sciences Meeting (National Harbor, MD), American Institute of Aeronautics and Astronautics, Reston, VA, 2014, (submitted for publication).
- ¹⁵Guo, Y., Czech, M.J., and Thomas, R.H., "Open Rotor Noise Shielding by Blended-Wing-Body Aircraft," 19th AIAA/CEAS Aeroacoustics Conference (Berlin, Germany), American Institute of Aeronautics and Astronautics, Reston, VA, 2013, (submitted for publication).
- ¹⁶Thomas, R.H., Burley, C.L., Lopes, L.V., Bahr, C.J., Gern, F.H., and Van Zante, D.E., "System Noise Assessment and the Potential for a Low Noise Hybrid Wing Body Aircraft with Open Rotor Propulsion," 52nd Aerospace Sciences Meeting (National Harbor, MD), American Institute of Aeronautics and Astronautics, Reston, VA, 2014, (submitted for publication).
- ¹⁷Guo, Y. and Thomas, R.H., "System Noise Assessment of Blended-Wing-Body Aircraft with Open Rotor Propulsion," 19th AIAA/CEAS Aeroacoustics Conference (Berlin, Germany), American Institute of Aeronautics and Astronautics, Reston, VA, 2013, (submitted for publication).
- ¹⁸Liebeck, R.H., "Design of the Blended-Wing-Body Subsonic Transport," AIAA Paper No. 2002-0002.
- ¹⁹Jones, M.J., private communication, 2010.

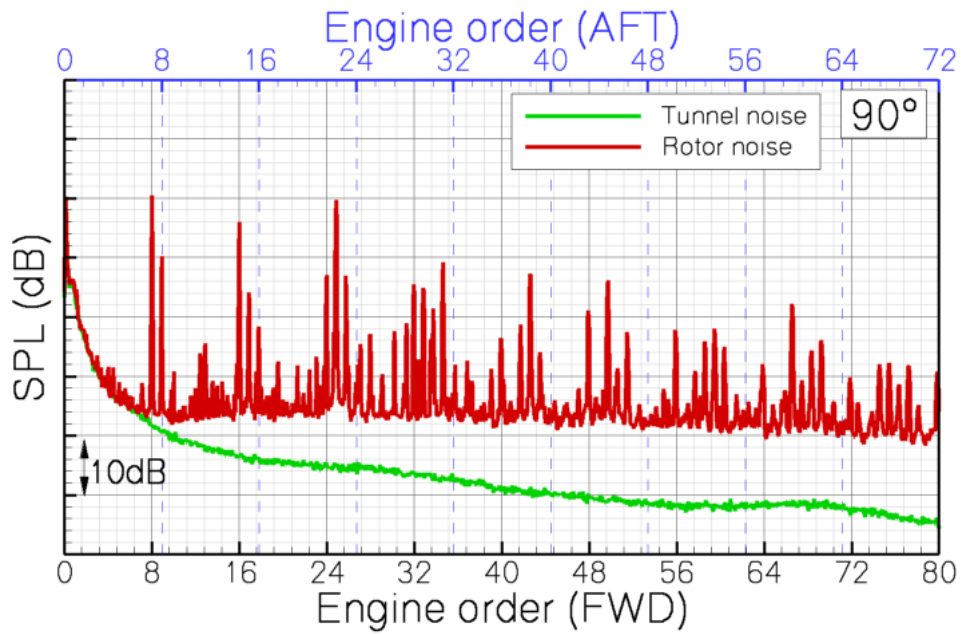


Figure 11. Open rotor spectrum relative to background wind tunnel noise.

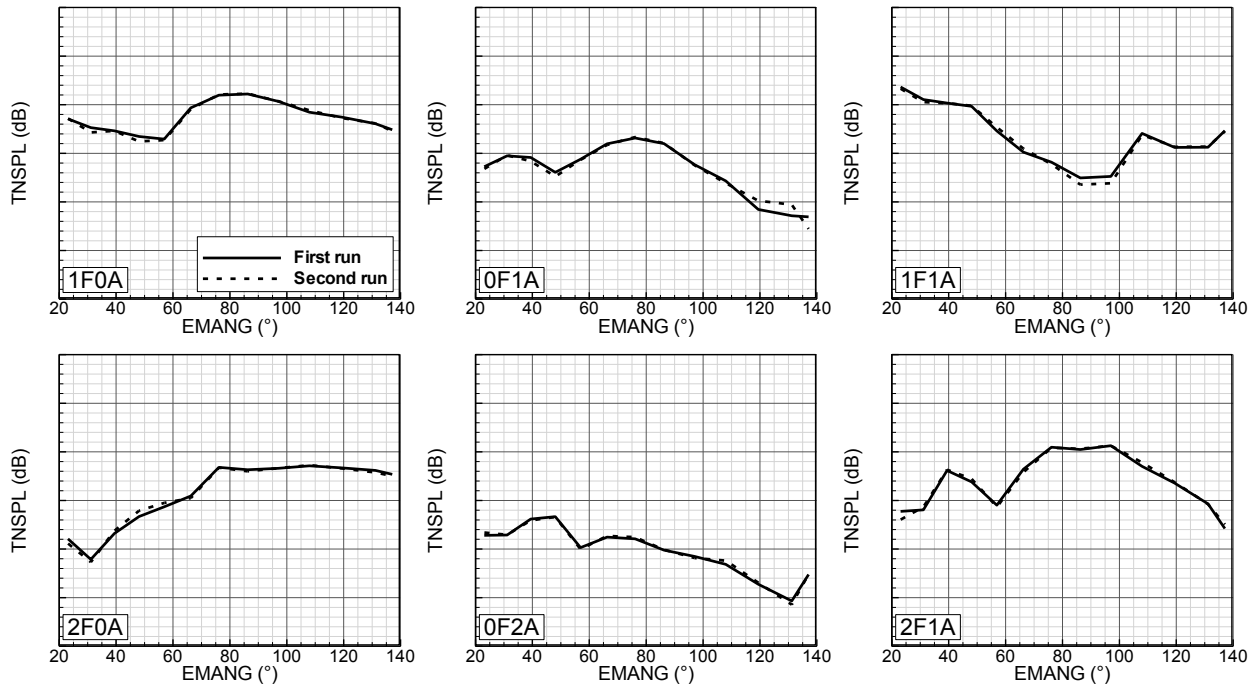


Figure 12. Typical repeatability of dominant modes at low power. Spacing between major gridlines is 10dB.

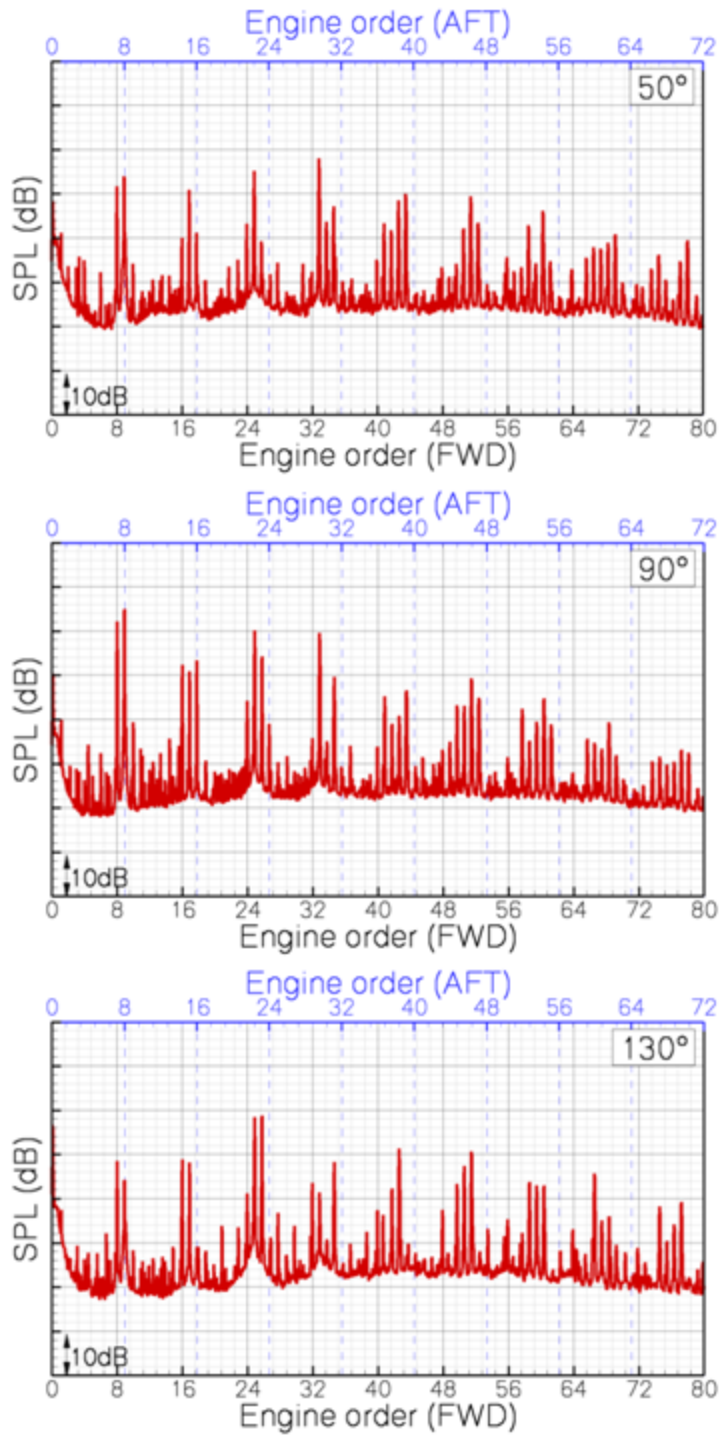


Figure 13. Open rotor spectrum (as a function of engine order) for the isolated open rotor at different polar angles.

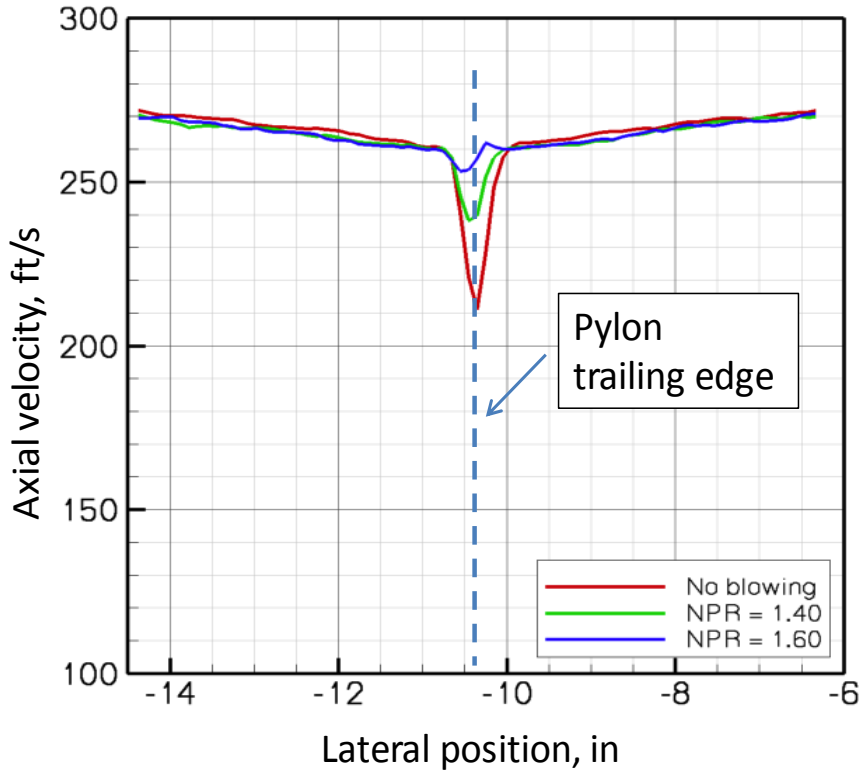


Figure 14. Axial velocity downstream of the pylon versus lateral position for different pylon blowing settings.

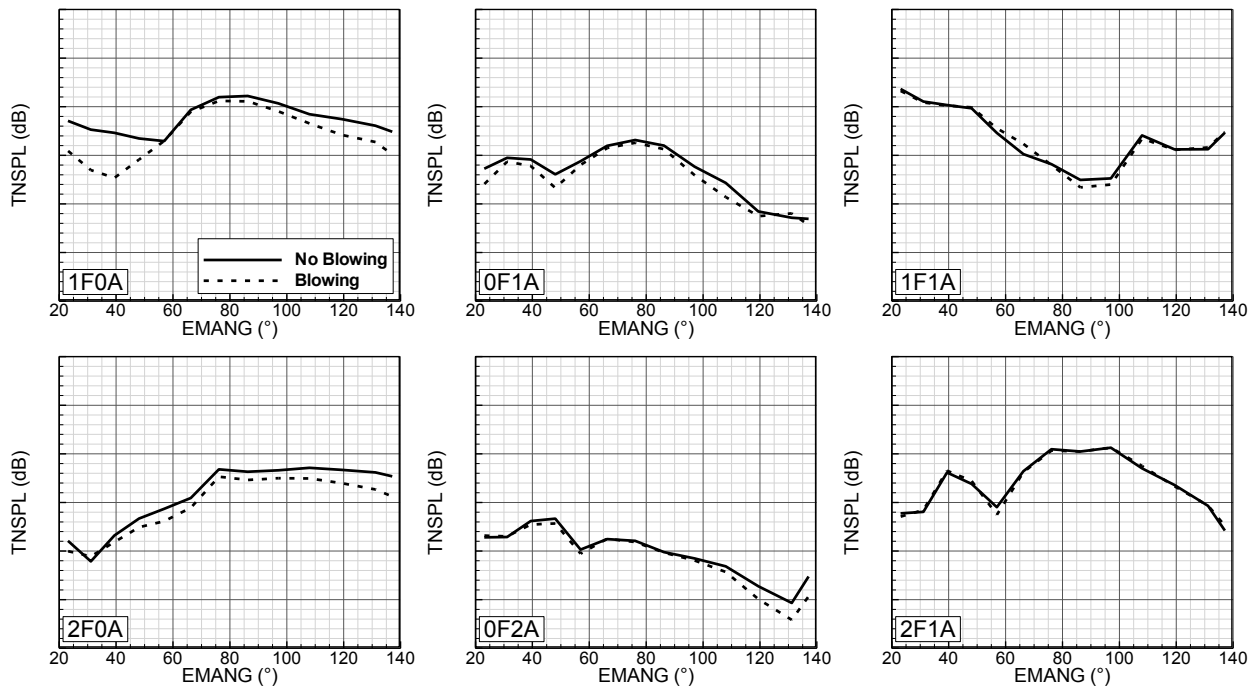


Figure 15. Comparison of tone levels for pylon with (dashed lines) and without (solid lines) blowing. Spacing between major gridlines is 10dB.

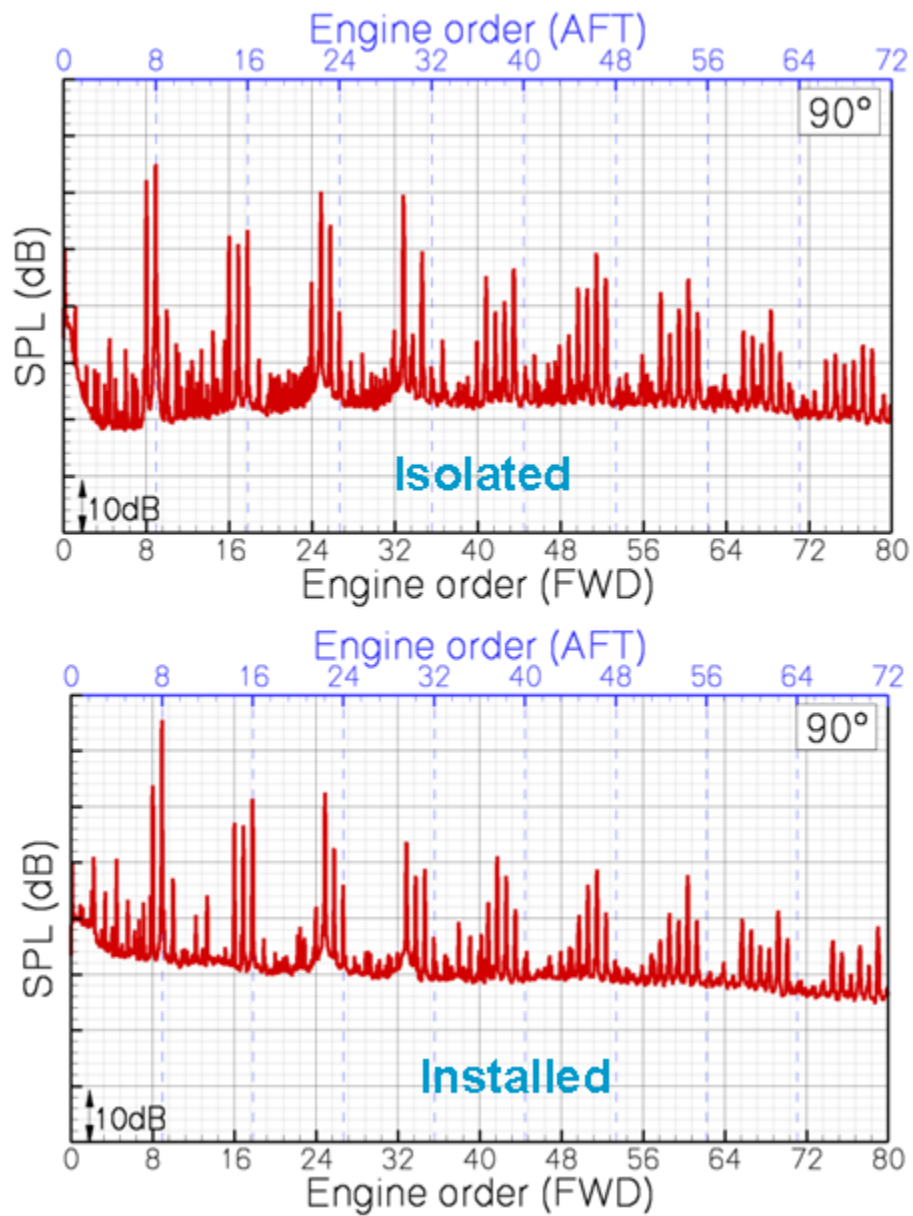


Figure 16. Open rotor spectrum, isolated, and then with the open rotor positioned forward of the conventional wing.

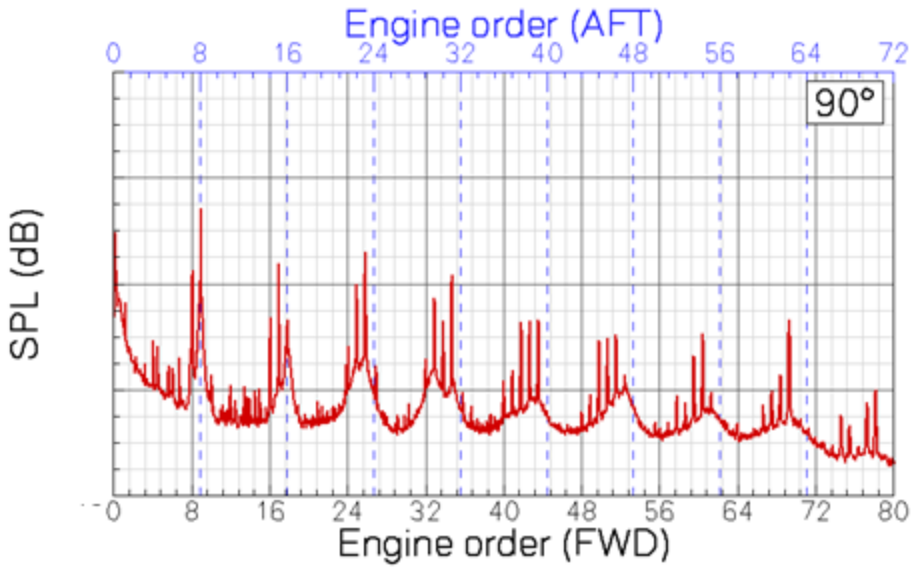


Figure 17. Open rotor spectrum for an installation at a wing mid-chord location. Gridlines are 20dB apart (same reference level as in Figure 16 for isolated data above).

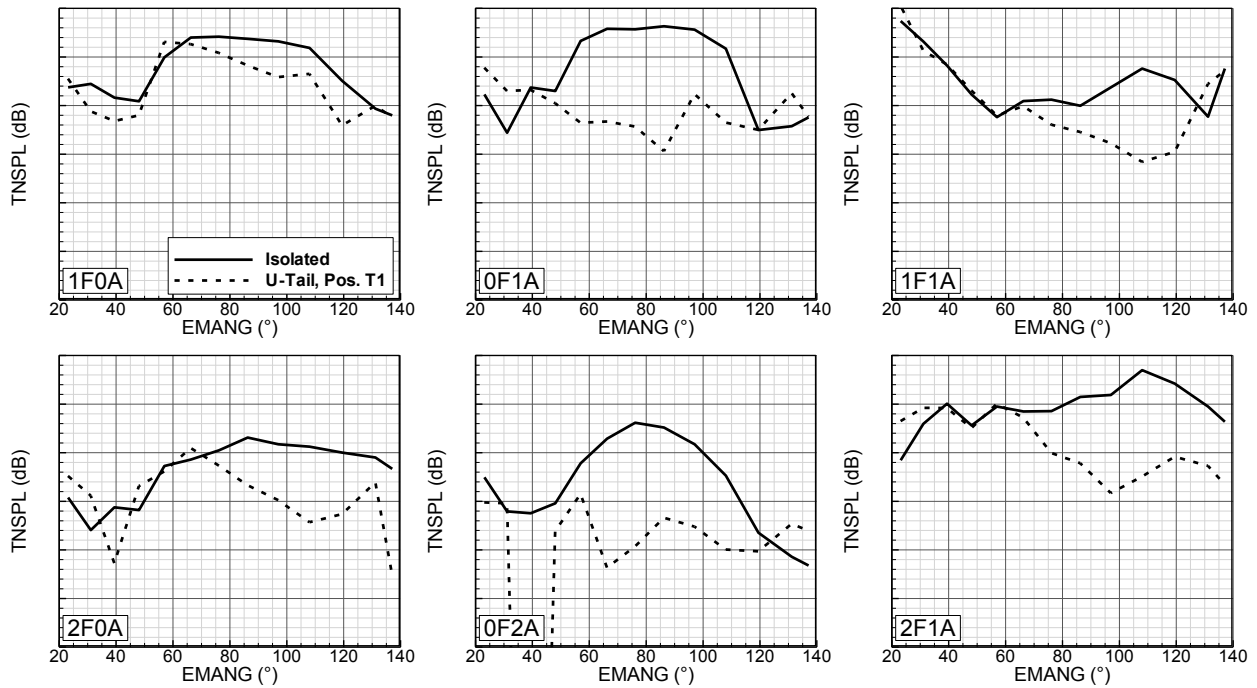


Figure 18. The installation effects of a tube and wing configuration with a U-Tail installed as shown in Figure 7. Spacing between major gridlines is 10dB.

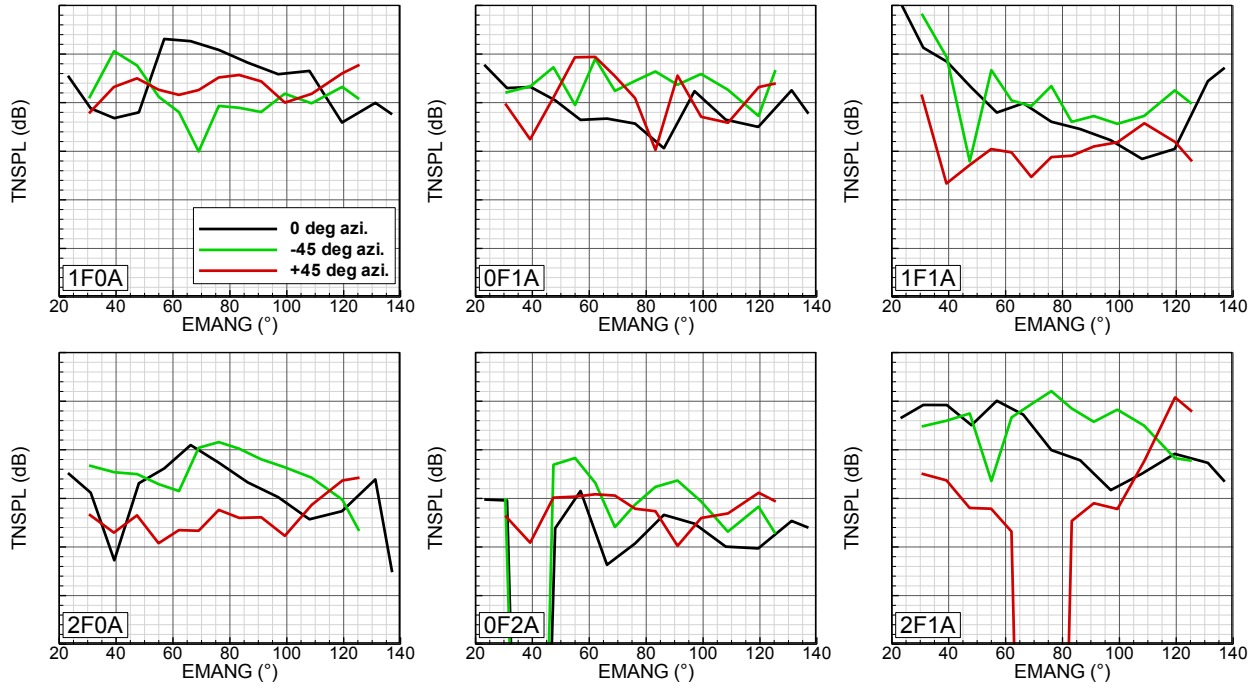


Figure 19. The azimuthal variation of the an open rotor when installed with a U-tail. Spacing between major gridlines is 10dB.

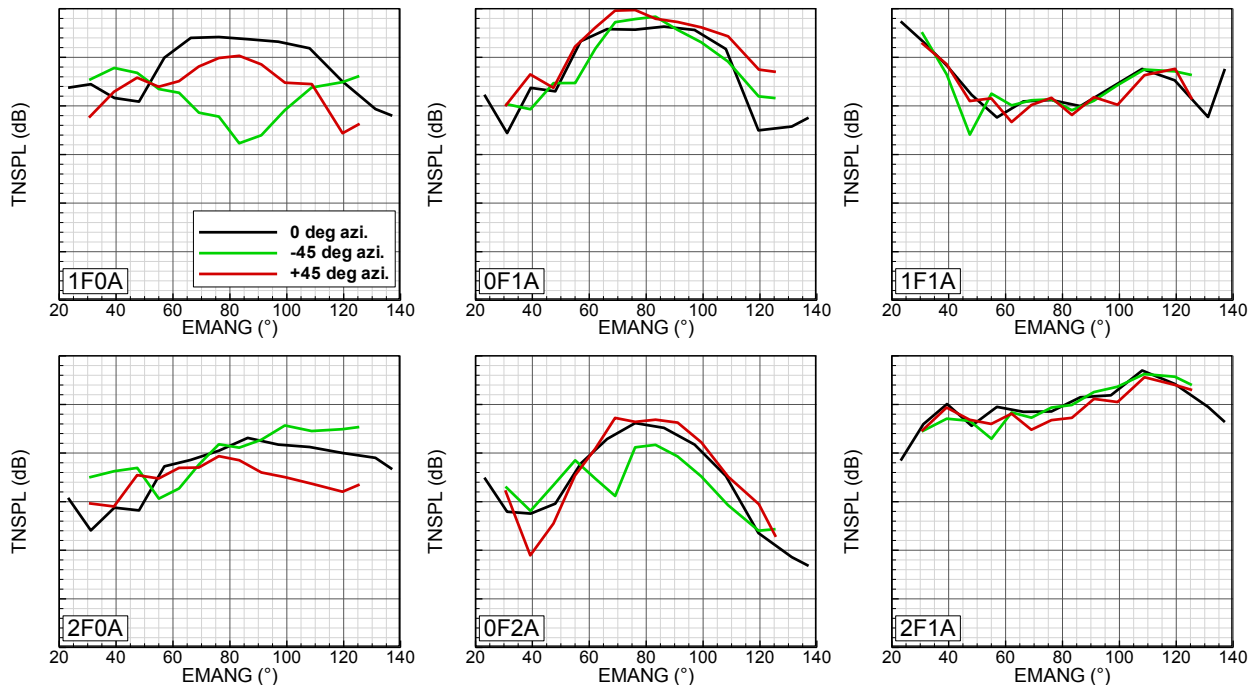


Figure 20. The azimuthal variation of the open rotor in an isolated set-up. Spacing between major gridlines is 10dB.

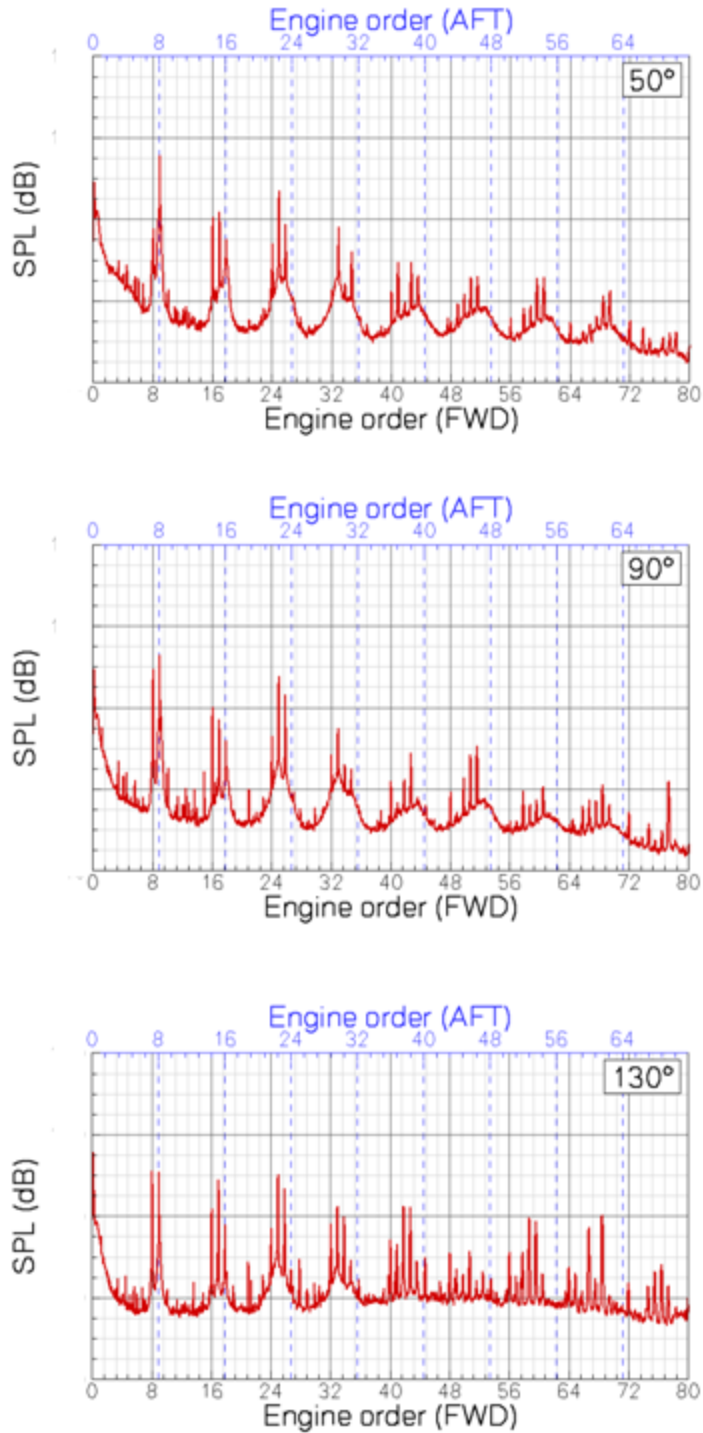


Figure 21. Open rotor spectra with the BWB airframe. The rotor is at 1D upstream of the trailing edge (no verticals, no lining). Same reference level as in Figure 16 for isolated data above. Spacing between major gridlines is 20dB.

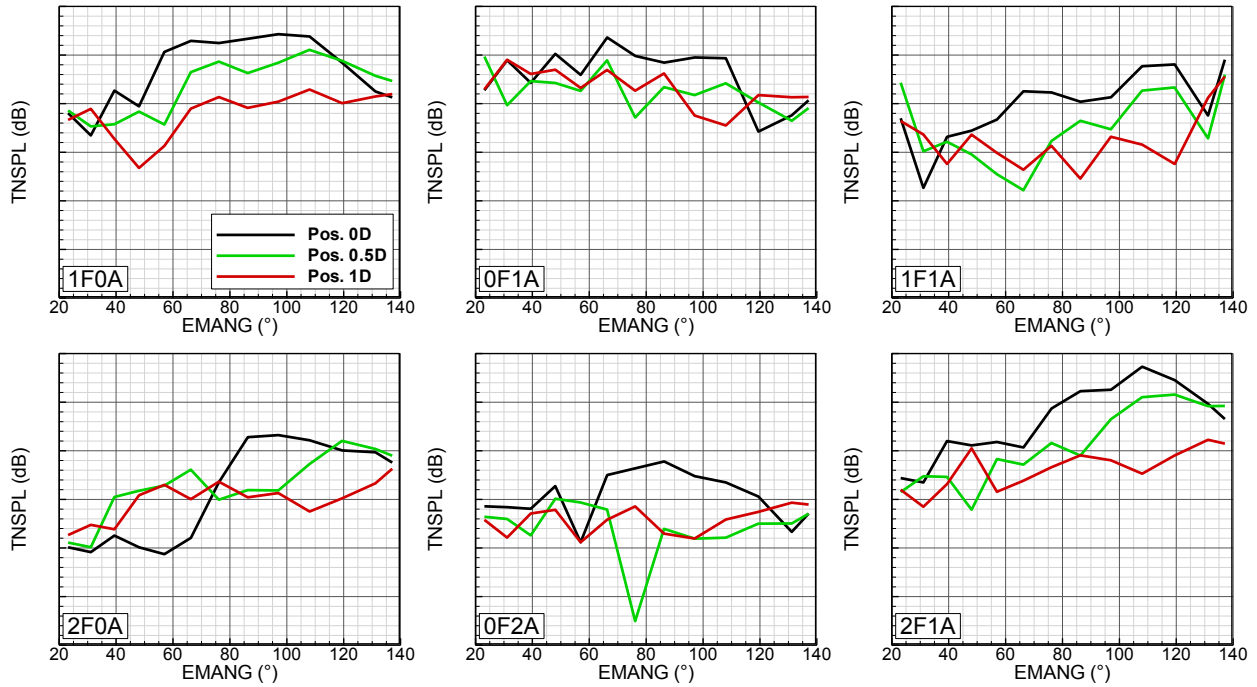


Figure 22. Variation of shielding effects with open rotor position relative to HWB trailing edge. Spacing between major gridlines is 10dB.

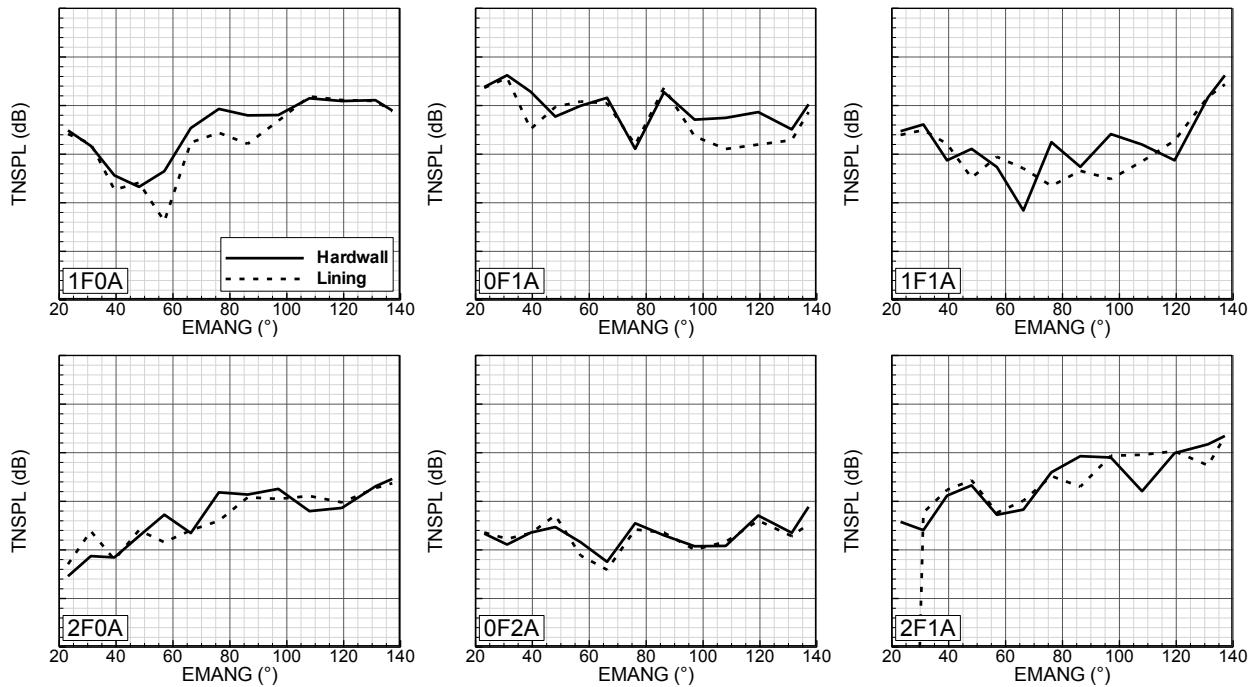


Figure 23. The HWB with lining in the wing pocket and the elevons (thin line) compared to the hard walled baseline HWB. The open rotor is positioned at 1D.

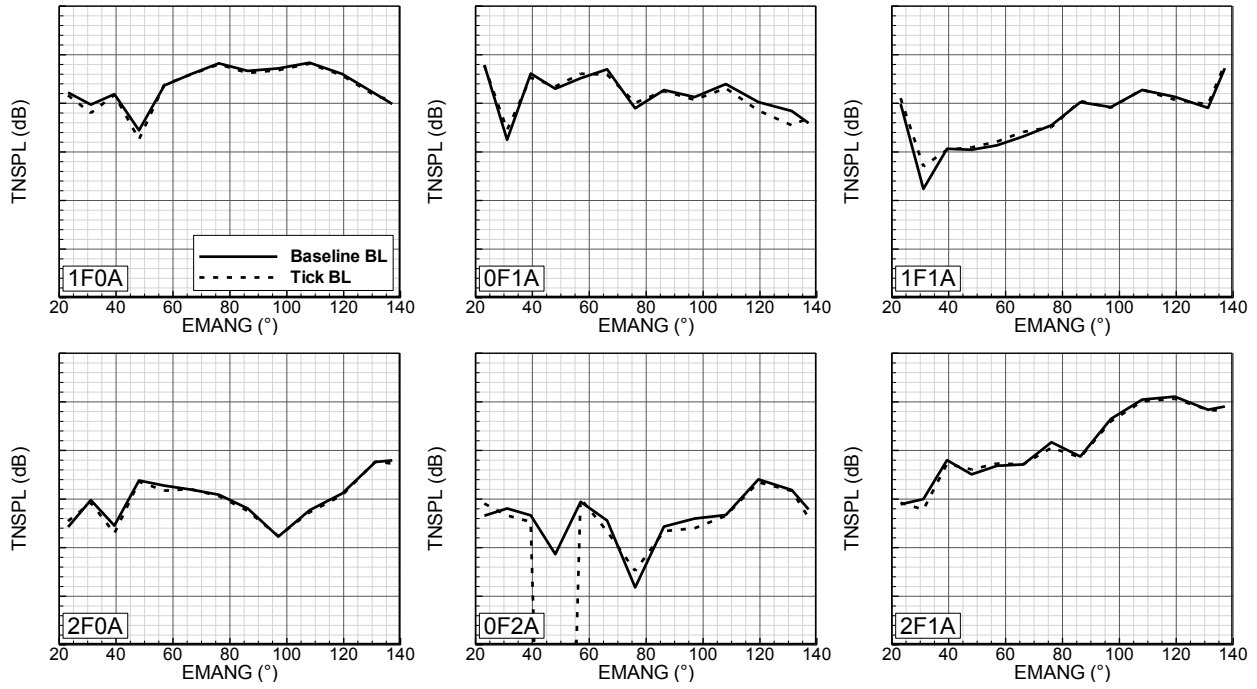


Figure 24. The effect of boundary layer thickness when comparing the baseline ($\delta \sim 0.5''$) to a thick boundary layer ($\delta \sim 2.0''$).

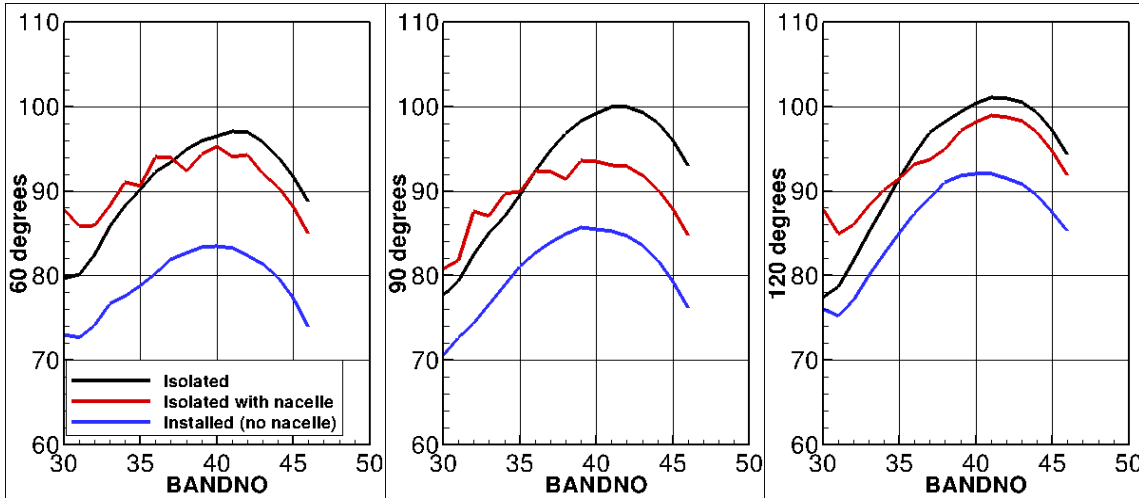


Figure 25. Variation of the broadband noise source levels with set-up and polar angle.